



## Negative Spin Exchange in a Multielectron Quantum Dot

Frederico Martins,<sup>1</sup> Filip K. Malinowski,<sup>1</sup> Peter D. Nissen,<sup>1</sup> Saeed Fallahi,<sup>2</sup> Geoffrey C. Gardner,<sup>2</sup> Michael J. Manfra,<sup>2,3</sup> Charles M. Marcus,<sup>4</sup> and Ferdinand Kuemmeth<sup>1</sup>

<sup>1</sup>*Center for Quantum Devices, Niels Bohr Institute, University of Copenhagen, 2100 Copenhagen, Denmark*

<sup>2</sup>*Department of Physics and Astronomy, Station Q Purdue, and Birck Nanotechnology Center, Purdue University, West Lafayette, Indiana 47907, USA*

<sup>3</sup>*School of Electrical and Computer Engineering and School of Materials Engineering, Purdue University, West Lafayette, Indiana 47907, USA*

<sup>4</sup>*Center for Quantum Devices and Station Q Copenhagen, Niels Bohr Institute, University of Copenhagen, 2100 Copenhagen, Denmark*

(Received 3 June 2017; published 30 November 2017)

We use a one-electron quantum dot as a spectroscopic probe to study the spin properties of a gate-controlled multielectron GaAs quantum dot at the transition between odd and even occupation numbers. We observe that the multielectron ground-state transitions from spin-1/2-like to singletlike to tripletlike as we increase the detuning towards the next higher charge state. The sign reversal in the inferred exchange energy persists at zero magnetic field, and the exchange strength is tunable by gate voltages and in-plane magnetic fields. Complementing spin leakage spectroscopy data, the inspection of coherent multielectron spin exchange oscillations provides further evidence for the sign reversal and, inferentially, for the importance of nontrivial multielectron spin exchange correlations.

DOI: 10.1103/PhysRevLett.119.227701

Semiconducting quantum dots with individual unpaired electronic spins offer a compact platform for quantum computation [1–8]. In these approaches, the essential role of nearest-neighbor interactions poses technological challenges to upscaling, due to the density of electrodes that define and control these quantum circuits [9–13]. This issue has stimulated efforts to study long-range coupling of spin qubits either by electrical dipole-dipole interaction [12–14] or via superconducting microwave cavities [15–17]. However, these approaches involve the charge degree of freedom, which makes the qubit susceptible to electrical noise [18–21]. Alternatively, pulses that induce exchange interactions can be performed fast in a charge-insensitive manner [21–24]. Even though the exchange interaction is intrinsically short-ranged, its range can be increased by means of a quantum mediator [25,26]. In particular, using a large multielectron quantum dot as an exchange mediator has the potential to do both: provide fast spin interaction [27,28] and alleviate spatial control line crowding.

Here we investigate a GaAs multielectron quantum dot and show that its spin properties make it suitable for use as a coherent spin mediator. The experiment involves three quantum dots that can be detuned relative to each other using top-gate voltage pulses. The central one-electron dot serves as a probe: Its spin can be tunnel coupled either to the left one-electron dot (serving as a reference spin for initialization and readout) or to a large dot on the right, thereby probing its multielectron spin states. We focus on a particular occupancy of the multielectron dot that we find to be odd,  $2N + 1$ , and characterized by an effective spin  $1/2$ . We establish that the exchange coupling between the

central probe spin and the multielectron spin depends strongly and nonmonotonically on the detuning of relevant gate voltages. Remarkably, this exchange coupling becomes negative, i.e., triplet preferring, as the central electron is transferred into the right dot. We therefore infer a spin-1 ground state for  $2N + 2$  occupation, even in the absence of an applied magnetic field. Besides fundamental implications for the role of nontrivial interactions within a multielectron dot, presented elsewhere for a large range of dot occupations [29], our finding has practical applications. For example, the nonmonotonicity of the exchange profile results in a sweet spot at which the exchange splitting has a reduced susceptibility to charge noise. Meanwhile, the sign reversal removes a constraint for the construction of compact dynamically corrected exchange gates [30,31].

The three quantum dots were fabricated in a GaAs/Al<sub>0.3</sub>Ga<sub>0.7</sub>As heterostructure hosting a high-mobility two-dimensional electron gas with a bulk density  $n = 2.5 \times 10^{15} \text{ m}^{-2}$ . The confining potential and dot occupancy is voltage-tuned by metallic gates [8,21]. Figure 1(a) shows the two accumulation gates (colored in green) surrounded by depletion gates and a schematic cut through the resulting triple-well potential. Gates labeled  $V_{L/M/R}$  (colored in red) are connected to high-bandwidth coaxial lines and allow the application of nanosecond-scale voltage pulses. An adjacent quantum dot (not shown) serves as a fast charge sensor, i.e., changes in its conductance change the amplitude ( $V_{rf}$ ) of a reflected rf carrier [32]. All measurements were conducted at the base temperature of a dilution refrigerator.

The device can be viewed as a two-electron double quantum dot (DQD) tunnel-coupled to a multielectron dot

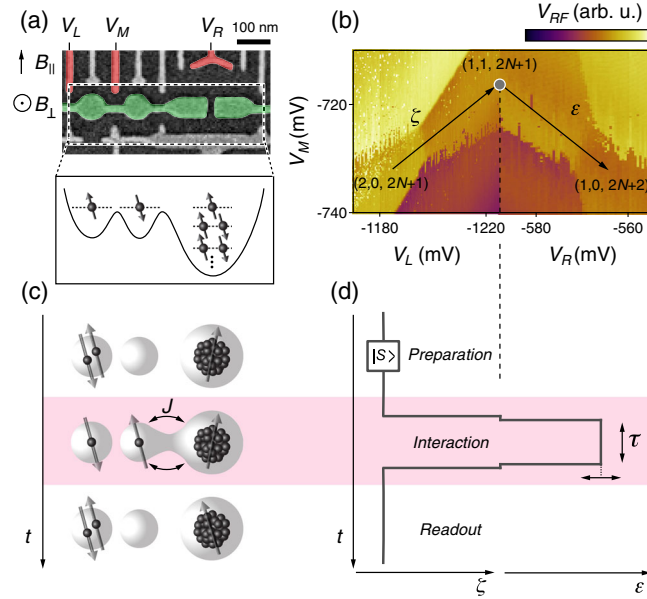


FIG. 1. (a) Electron micrograph of the device consisting of a two-electron double quantum dot next to a multi-electron quantum dot. The accumulation gate (colored in green) is operated at a positive voltage. Remaining gates deplete the underlying two-dimensional electron gas. Gates  $V_{L/M/R}$ , highlighted in red, are connected to high-bandwidth lines. (b) Charge diagrams indicating the electron occupation of the triple quantum dot as a function of  $V_{L/M/R}$ . Arrows indicate  $\zeta$  and  $\epsilon$  axes in gate voltage space. (c) Concept of the experiment. Two electrons are initialized in a singlet state in the left quantum dot. Thereafter, one of the electrons is moved to the middle dot and interacts with the multi-electron quantum dot through exchange interaction  $J$ . At the end, readout is attained by performing a spin-to-charge conversion for two-electron spin states in the double quantum dot. (d) Implementation of the pulse sequence in terms of  $\zeta$  and  $\epsilon$ .

(MED) with an estimated number of electrons between 50 and 100, based on  $n$  and the area of the MED. By measuring  $V_{rf}$  as a function of voltages  $V_{L/M/R}$ , we map out the dots' occupancies in the vicinity of the charge states  $(2, 0, 2N + 1)$ ,  $(1, 1, 2N + 1)$ , and  $(1, 0, 2N + 2)$ . Here, the numbers correspond to electron occupation in the left dot, the central dot, and the MED, respectively. The resulting charge diagram in Fig. 1(b) allows the definition of two detuning axes in gate-voltage space,  $\zeta$  and  $\epsilon$ , crossing at the point indicated by the gray circle. A reduction of  $\zeta$  pushes the central electron into the left dot, whereas an increase in  $\epsilon$  pushes it to the MED (cf. arrows).

The MED spin states are probed by the pulse sequence illustrated in Figs. 1(c) and 1(d). First, two electrons are prepared in the left dot in a singlet state, by pulsing to the  $(2, 0, 2N + 1)$  charge state. Then a  $\zeta$  pulse to the  $(1, 1, 2N + 1)$  state turns off intra-DQD exchange interactions while maintaining the two-electron spin state. The next step probes the interaction between the central electron and the MED in the vicinity of the charge transition between  $(1, 1, 2N + 1)$  and  $(1, 0, 2N + 2)$ . This is done by pulsing

$\epsilon$ , i.e., by temporarily applying a negative voltage pulse to  $V_M$  and a positive voltage pulse to  $V_R$ . After an interaction time  $\tau$ , we return to  $(1, 1, 2N + 1)$  and immediately reduce  $\zeta$  for a single-shot reflectometry readout [33]: If  $V_{rf}$  indicates a  $(2, 0, 2N + 1)$  charge state, we assign a singlet outcome, whereas  $(1, 1, 2N + 1)$  indicates that a spin interaction with the MED has occurred (resulting in a two-electron triplet state, which is spin blocked).

Leakage spectroscopy is performed by choosing  $\tau = 150$  ns sufficiently long to detect incoherent spin mixing between the central electron and MED states. Figure 2(a) shows the probability of a singlet outcome,  $P_S(\epsilon, B_{\parallel})$ , where  $\epsilon$  is the detuning voltage during the interaction step and  $B_{\parallel}$  is the applied in-plane magnetic field [see the arrow in Fig. 1(a)]. To make a connection to the conventional two-electron DQD regime, we also plot  $P_S(\zeta, B_{\parallel})$ , acquired by replacing the composite  $\zeta - \epsilon$  pulse in Fig. 1(d) by a pure  $\zeta$  pulse. Incoherent leakage from the initialized singlet state is observed as a sharp suppression of  $P_S$  for particular detuning values, with a nontrivial magnetic field dependence for  $\epsilon > -5$  mV. To understand this spectrum, we note that all features below  $\epsilon \approx -5$  mV are well explained by mixing with fully polarized spin states, consistent with previous spin leakage experiments: The  $\zeta$  dependence (marked by a white triangle) is analogous to mixing between a singlet and  $|\uparrow\uparrow\rangle \equiv \uparrow\uparrow$  in two-electron DQDs [7,9,34], whereas the  $\epsilon$  dependence (blue triangle) is analogous to mixing between a singletlike state and  $|\uparrow\uparrow\uparrow\rangle$  in three-electron triple quantum dots [35]. (Here, each arrow indicates the spin state within one quantum dot.) The characteristic dependence on  $B_{\parallel}$  arises from the Zeeman shift of fully polarized spin states and a nonlinear detuning dependence of  $J$  [36,37].

This identification suggests an odd multi-electron occupation, i.e.,  $(1, 1, 2N + 1)$ , with effective spin  $1/2$ . Accordingly, we interpret the continuation of the main leakage feature (indicated by a black dot) as the degeneracy point of  $|\uparrow\rangle|S\rangle$  and  $|\uparrow\uparrow\uparrow\rangle$ . In other words, the position of this feature indicates the detuning at which the exchange interaction  $J$  equals the Zeeman splitting  $|g|\mu_B B_{\parallel}$  (here  $g = -0.44$  is the electronic  $g$  factor for GaAs and  $\mu_B$  is the Bohr magneton), thereby allowing us to quantify the exchange splitting between the central spin and the effective MED spin [Fig. 2(c)]. Towards higher detuning,  $\epsilon > -5$  mV in Fig. 2(a), an overall drop in the background of  $P_S$  indicates that the MED ground-state transitions into  $(1, 0, 2N + 2)$ , approximately concurrent with the sharp leakage feature (blue triangle) reaching a maximum before turning towards  $B_{\parallel} = 0$  (black dot). We interpret this maximum as a maximum in the exchange profile,  $J(\epsilon)$ , and associate the crossing at  $B_{\parallel} = 0$  with a sign reversal of  $J(\epsilon)$ . At  $\epsilon = 0$  two additional leakage features appear at  $B_{\parallel} = 0$ . One is nearly field independent (magenta diamond), and hence we associate it with the crossing between  $|\uparrow\rangle|S\rangle$  and  $|\uparrow\rangle|T_0\rangle$ , which has the same spin projection in the direction of the magnetic field. The other feature (green square) indicates a crossing

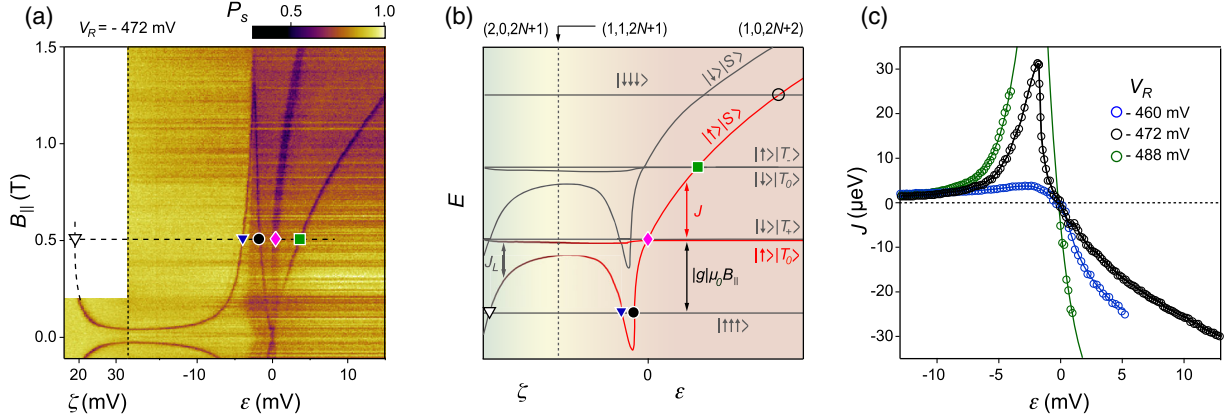


FIG. 2. (a)  $P_S$  as a function of  $\zeta$ ,  $\epsilon$ , and  $B_{||}$  for a fixed, long interaction time  $\tau = 150$  ns. The vertical dashed line indicates the crossing of  $\zeta$  and  $\epsilon$  axes in Fig. 1(b). (b) Corresponding energy diagram of the spin states of a Heisenberg model, as a function of  $\zeta$  and  $\epsilon$  for a fixed  $B_{||}$ . States highlighted in red witness the interaction between the central probe spin and the effective MED spin, which combine into a singletlike state,  $|\uparrow\rangle|S\rangle$ , that is above a tripletlike state,  $|\uparrow\rangle|T_0\rangle$ , for sufficiently large  $\epsilon$  (negative  $J$ ). The charge character of the ground-state transitions from  $(2, 0, 2N + 1)$  via  $(1, 1, 2N + 1)$  to  $(1, 0, 2N + 2)$  as indicated by the background shading. The sign reversal of  $J$  happens at  $\epsilon = 0$ . The Zeeman shift  $|g|\mu_B B_{||}$  and crossings with other states leading to spin leakage features in (a) are indicated (see the main text). Leakage from  $|\uparrow\rangle|S\rangle$  to the fully polarized  $|\downarrow\downarrow\downarrow\rangle$  state (empty circle) is not observed in (a), because weak Overhauser gradients or spin-orbit coupling do not allow such large changes in spin projection. (c) Experimental exchange profiles for different operating points (distortions of the confining potential), identified by  $V_R$  during the readout step (symbols). Black circles are extracted from (a). Solid lines are guides to the eye.

with  $|\uparrow\rangle|T_{-}\rangle$ . Since the energy of this state increases for a larger magnetic field,  $J$  must change sign.

To support this analysis by a full spin spectrum, we impose the inferred exchange profile  $J(\zeta, \epsilon)$  from Fig. 2(c) on a Heisenberg model of three spin-1/2 orbitals [38]. The resulting energy diagram, sketched in Fig. 2(b) for finite  $B_{||}$ , allows us to identify all characteristic leakage features. On the left side of the energy diagram, only tunneling across the left barrier is significant (giving rise to intra-DQD exchange coupling  $J_L$ ), and the eigenstates are the tensor products of a DQD spin state and a MED “spectator” spin. For example, the white triangle marks the crossing between  $|S\rangle|\uparrow\rangle$  and  $|\uparrow\uparrow\uparrow\rangle$  and relates the leakage feature in (a) to  $J_L(\zeta)$ . Analogously, on the right side of the energy diagram, the left dot is decoupled and hosts the spectator spin, while the central spin interacts with the effective MED spin. Here, field-dependent crossings map out the positive (blue and black) and negative (green marker) regimes of  $J(\epsilon)$ . In particular, for crossings of  $|\uparrow\rangle|S\rangle$  with  $|\uparrow\uparrow\uparrow\rangle$ ,  $|\uparrow\rangle|T_0\rangle$  and  $|\uparrow\rangle|T_{-}\rangle$  rapid mixing is expected to occur [39]. Thereby, the Heisenberg model qualitatively explains all features in the observed leakage spectrum. At a high magnetic field, however, the observed leakage feature indicated with a magenta diamond is not field independent as predicted by the model, likely due to orbital coupling of  $B_{||}$  to MED states.

In contrast to three-electron triple dots [35,40], where  $J$  is always positive, we observe that  $|\uparrow\rangle|S\rangle$  and  $|\uparrow\rangle|T_0\rangle$  cross each other at a particular detuning value (which we used to define  $\epsilon = 0$ ). This implies that the exchange interaction between the single and multielectron quantum dot changes

sign from positive to negative; i.e., it is singlet preferring for small hybridization and becomes triplet preferring once the central electron has transferred to the MED. Next, we test for robustness and gate-tunability of this effect. In Fig. 2(c), we plot  $J(\epsilon)$  extracted from Fig. 2(a) (black symbols) and compare it to two exchange profiles (green and blue symbols) measured by distorting the confining potential while preserving the charge configuration of the triple dot system (cf. Supplemental Fig. S1 [41]). In all cases,  $J(\epsilon)$  shows the same behavior, namely, a maximum and sign reversal in the vicinity of the charge transition and a negative sign in the  $(1, 0, 2N + 2)$  configuration. This interpretation implies that the  $2N + 2$  charge state of the MED has a total spin of 1 at zero magnetic field, which is further confirmed by studying the MED behavior over multiple charge states [29].

Complementary evidence for the sign reversal in  $J$  is obtained from time-domain measurements. To this end, we induce coherent exchange oscillations between the central and MED spin by significantly reducing (and varying) the interaction time  $\tau$ . The observed oscillations are analogous to those observed in exchange-only qubits [36,40], where the rate of phase accumulation between its two qubit states [i.e., frequency of  $P_S(\tau)$ ] is a measure of the exchange splitting  $|J|$ . However, the observed pattern of  $P_S(\epsilon, \tau)$ , shown in Fig. 3(a) for the same dc tuning parameters as in Fig. 2(a), differ from that of exchange-only qubits. The appearance of a chevronlike pattern around  $\epsilon = -2$  mV indicates the presence of a local maximum in  $|J(\epsilon)|$ : Following contours of equal phase ( $\phi$ ) around this “sweet spot,” we note that for constant  $\tau\phi(\epsilon)$  first increases and



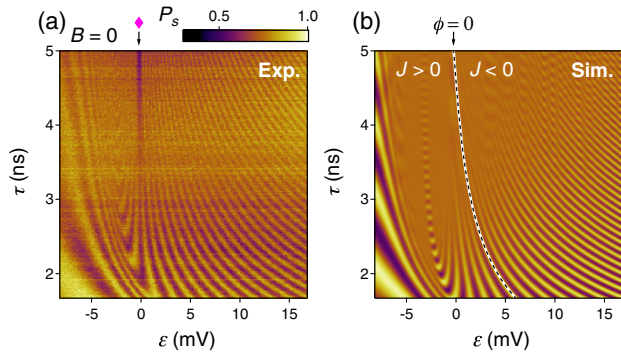


FIG. 3. (a) Exchange oscillations in  $P_S$  as a function of  $\varepsilon$  and exchange time  $\tau$ , in the vicinity of the  $(1, 1, 2N + 1)$  and  $(1, 0, 2N + 2)$  charge transition. The external magnetic field is zero, and dc tuning voltages are the same as in Fig. 2(a) ( $V_R = 472$  mV). (b) Simulated exchange oscillations, assuming  $J(\varepsilon)$  from Fig. 2(c), Gaussian low-frequency noise in  $\varepsilon$  with a standard deviation of 0.18 mV, and a rise time of the experimental instrumentation of 0.8 ns. A contour with no net accumulated phase,  $\phi = 0$ , divides operating regimes where  $J$  is positive and negative. Leakage out of the simulated subspace [magenta diamond in (a); see the text] was ignored in the simulation.

then decreases. It continues to do so smoothly beyond the  $\phi = 0$  contour, implying a sign reversal in  $J(\varepsilon)$ . Additionally, for large  $\tau$  a dark feature appears at  $\varepsilon = 0$  (magenta diamond), which for  $\tau \rightarrow 150$  ns turns into the incoherent leakage feature discussed in Fig. 2(a).

To show consistency between time-domain and leakage spectroscopy results, we perform numerical simulations of the exchange oscillations using the measured exchange profile presented in Fig. 2(c). The simulation is limited to the state space with total spin  $S = 1/2$  and spin projection  $S_z = 1/2$  on the direction of the external magnetic field [indicated with red in Fig. 2(b)] and includes a quasistatic Gaussian noise in  $\varepsilon$  with standard deviation  $\sigma_\varepsilon = 0.18$  mV [21,42] and a rise time of our instrumentation of 0.8 ns. The simulation reproduces a chevron pattern [Fig. 3(b)], whereas simulations using  $J(\varepsilon) = |J(\varepsilon)|$  produce a qualitatively different pattern (not shown). Therefore, the contour  $\phi = 0$  does indeed separate regions with  $J > 0$  from regions with  $J < 0$ .

Finally, we study the effects of applied magnetic fields on the exchange profile. Figure 4(a) presents  $P_S$  as a function of  $\varepsilon$  and out-of-plane magnetic field  $B_\perp$ , while keeping  $B_\parallel = 0$  and  $\tau = 3.33$  ns fixed. In such a plot, contours correspond to constant  $J$  in the  $\varepsilon$ - $B_\perp$  plane, and their curvature indicates that out-of-plane magnetic fields move the sign reversal of  $J$  towards higher detuning (cf.  $\phi = 0$  contour, marked by a dashed line). For comparison, within the same range,  $B_\parallel$  has no observable influence on the pattern of the exchange oscillations [Fig. 4(b)]. By choosing  $\tau$  longer than the coherence time, we obtain the  $B_\perp$  dependence of the leakage spectrum [Fig. 4(c), using  $\tau = 150$  ns]. The two leakage features appearing for negative values of  $\varepsilon$  correspond to mixing between  $|\uparrow\rangle|S\rangle$  and the fully polarized  $|\uparrow\uparrow\uparrow\rangle$ . The leakage

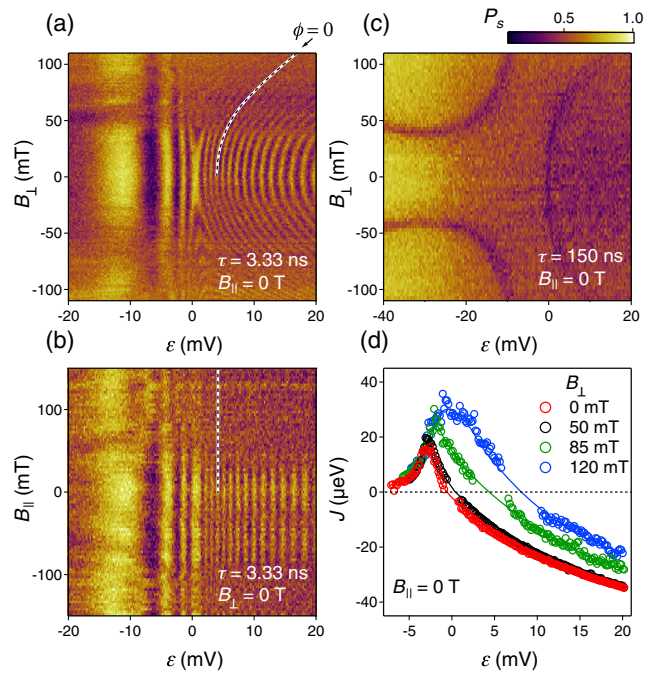


FIG. 4. (a) Exchange oscillations as a function of  $B_\perp$  and  $\varepsilon$  for fixed exchange time  $\tau = 3.33$  ns and fixed  $B_\parallel = 0$  T. (b) Exchange oscillations as a function of  $B_\parallel$  and  $\varepsilon$  for fixed exchange time  $\tau = 3.33$  ns and fixed  $B_\perp = 0$  T. (c) The same as (a) but in the leakage spectroscopy regime ( $\tau = 150$  ns). Features of reduced  $P_S$  correspond to mixing between  $|\uparrow\rangle|S\rangle$  and various other states [cf. horizontal cut of Fig. 2(a) at  $B_\parallel = 0$ ]. A small deviation between the  $J = 0$  feature in (c) and the  $\phi = 0$  contour in (a) is likely due to the very different values of  $\tau$  in combination with finite-rise-time effects of our instrumentation. (d)  $J(\varepsilon)$  extracted for different values of  $B_\perp$ .

feature appearing for positive values of  $\varepsilon$  indicates  $J = 0$ ; similar to Fig. 2, we expect it to split into three lines at higher fields.

Exchange profiles  $J(\varepsilon)$  for  $B_\perp = 0, 50, 85,$  and  $120$  mT were extracted from  $P_S(\varepsilon, \tau)$  maps obtained for the same tuning voltages as in Fig. 4(a) (Supplemental Fig. S2 [41]). Figure 4(d) establishes an electrical sweet spot in  $J(\varepsilon)$  that can be precisely tuned by  $B_\perp$ , hinting at the role of the underlying electronic orbitals. However, their microscopic changes, and associated effects on the exchange profiles, remain outside the scope of our model.

In summary, we have investigated the exchange interaction between a two-electron double quantum dot and a multielectron dot. We find that the multielectron dot with odd occupation behaves as a spin-1/2 object that gives rise to a nonmonotonic exchange coupling to the neighboring dot. By changing the relative dot detuning voltage by a few millivolts, the sign of the exchange interaction can be tuned from positive to negative (also at zero magnetic field), indicating the presence of nontrivial electron-electron interactions. Finally, we show that the exchange profile can be tuned by either changing the gate potentials or applying an out-of-plane orbital magnetic field, giving rise

to a tunable electrical sweet spot that might benefit the implementation of high-fidelity exchange gates [21,24] in long-distance quantum mediators.

We thank Edwin Barnes, Stephen Bartlett, Andrew Doherty, and Thomas Smith for helpful discussions. This work was supported by LPS-MPO-CMTC, the EC FP7-ICT Project SiSPIN No. 323841, the Army Research Office, and the Danish National Research Foundation.

F. M. and F. K. M. contributed equally to this work.

- 
- [1] C. Kloeffer and D. Loss, *Annu. Rev. Condens. Matter Phys.* **4**, 51 (2013).
- [2] D. D. Awschalom, L. C. Bassett, A. S. Dzurak, E. L. Hu, and J. R. Petta, *Science* **339**, 1174 (2013).
- [3] D. Loss and D. P. DiVincenzo, *Phys. Rev. A* **57**, 120 (1998).
- [4] J. R. Petta, H. Lu, and A. C. C. Gossard, *Science* **327**, 669 (2010).
- [5] H. Bluhm, S. Foletti, I. Neder, M. Rudner, D. Mahalu, V. Umansky, and A. Yacoby, *Nat. Phys.* **7**, 109 (2011).
- [6] K. C. Nowack, F. H. L. Koppens, Y. V. Nazarov, and L. M. K. Vandersypen, *Science* **318**, 1430 (2007).
- [7] B. M. Maune, M. G. Borselli, B. Huang, T. D. Ladd, P. W. Deelman, K. S. Holabird, A. A. Kiselev, I. Alvarado-Rodriguez, R. S. Ross, A. E. Schmitz, M. Sokolich, C. A. Watson, M. F. Gyure, and A. T. Hunter, *Nature (London)* **481**, 344 (2012).
- [8] F. K. Malinowski, F. Martins, P. D. Nissen, E. Barnes, M. S. Rudner, S. Fallahi, G. C. Gardner, M. J. Manfra, C. M. Marcus, and F. Kuemmeth, *Nat. Nanotechnol.* **12**, 16 (2017).
- [9] M. Veldhorst, C. H. Yang, J. C. C. Hwang, W. Huang, J. P. Dehollain, J. T. Muhonen, S. Simmons, A. Laucht, F. E. Hudson, K. M. Itoh, A. Morello, and A. S. Dzurak, *Nature (London)* **526**, 410 (2015).
- [10] D. M. Zajac, T. M. Hazard, X. Mi, E. Nielsen, and J. R. Petta, *Phys. Rev. Applied* **6**, 054013 (2016).
- [11] T. Ito, T. Otsuka, S. Amaha, M. R. Delbecq, T. Nakajima, J. Yoneda, K. Takeda, G. Allison, A. Noiri, K. Kawasak, and S. Tarucha, *Sci. Rep.* **6**, 39113 (2016).
- [12] M. D. Shulman, O. E. Dial, S. P. Harvey, H. Bluhm, V. Umansky, and A. Yacoby, *Science* **336**, 202 (2012).
- [13] J. M. Nichol, L. A. Orona, S. P. Harvey, S. Fallahi, G. C. Gardner, M. J. Manfra, and A. Yacoby, *npj Quantum Inf.* **3**, 3 (2017).
- [14] L. Trifunovic, O. Dial, M. Trif, J. R. Wootton, R. Abebe, A. Yacoby, and D. Loss, *Phys. Rev. X* **2**, 011006 (2012).
- [15] X. Mi, J. V. Cady, D. M. Zajac, P. W. Deelman, and J. R. Petta, *Science* **355**, 156 (2017).
- [16] V. Srinivasa, J. M. Taylor, and C. Tahan, *Phys. Rev. B* **94**, 205421 (2016).
- [17] M. Russ and G. Burkard, *Phys. Rev. B* **91**, 235411 (2015).
- [18] W. A. Coish and D. Loss, *Phys. Rev. B* **72**, 125337 (2005).
- [19] J. M. Taylor, J. R. Petta, A. C. Johnson, A. Yacoby, C. M. Marcus, and M. D. Lukin, *Phys. Rev. B* **76**, 035315 (2007).
- [20] O. E. Dial, M. D. Shulman, S. P. Harvey, H. Bluhm, V. Umansky, and A. Yacoby, *Phys. Rev. Lett.* **110**, 146804 (2013).
- [21] F. Martins, F. K. Malinowski, P. D. Nissen, E. Barnes, S. Fallahi, G. C. Gardner, M. J. Manfra, C. M. Marcus, and F. Kuemmeth, *Phys. Rev. Lett.* **116**, 116801 (2016).
- [22] K. M. Weiss, J. M. Elzerman, Y. L. Delley, J. Miguel-Sanchez, and A. Imamoglu, *Phys. Rev. Lett.* **109**, 107401 (2012).
- [23] B. Bertrand, H. Flentje, S. Takada, M. Yamamoto, S. Tarucha, A. Ludwig, A. D. Wieck, C. Bauerle, and T. Meunier, *Phys. Rev. Lett.* **115**, 096801 (2015).
- [24] M. D. Reed, B. M. Maune, R. W. Andrews, M. G. Borselli, K. Eng, M. P. Jura, A. A. Kiselev, T. D. Ladd, S. T. Merkel, I. Milosavljevic, E. J. Pritchett, M. T. Rakher, R. S. Ross, A. E. Schmitz, A. Smith, J. A. Wright, M. F. Gyure, and A. T. Hunter, *Phys. Rev. Lett.* **116**, 110402 (2016).
- [25] T. A. Baart, T. Fujita, C. Reichl, W. Wegscheider, and L. M. K. Vandersypen, *Nat. Nanotechnol.* **11**, 330 (2016).
- [26] F. Braakman, P. Barthelemy, C. Reichl, W. Wegscheider, and L. M. K. Vandersypen, *Nat. Nanotechnol.* **8**, 432 (2013).
- [27] S. Mehl, H. Bluhm, and D. P. DiVincenzo, *Phys. Rev. B* **90**, 045404 (2014).
- [28] V. Srinivasa, H. Xu, and J. M. Taylor, *Phys. Rev. Lett.* **114**, 226803 (2015).
- [29] F. K. Malinowski, F. Martins, T. B. Smith, S. D. Bartlett, A. C. Doherty, P. D. Nissen, S. Fallahi, G. C. Gardner, M. J. Manfra, C. M. Marcus, and F. Kuemmeth, *arXiv:1710.10012*.
- [30] X. Wang, L. S. Bishop, J. P. P. Kestner, E. Barnes, K. Sun, and S. Das Sarma, *Nat. Commun.* **3**, 997 (2012).
- [31] X. Wang, L. S. Bishop, E. Barnes, J. P. Kestner, and S. Das Sarma, *Phys. Rev. A* **89**, 022310 (2014).
- [32] C. Barthel, M. Kjaergaard, J. Medford, M. Stopa, C. M. Marcus, M. P. Hanson, and A. C. Gossard, *Phys. Rev. B* **81**, 161308R (2010).
- [33] C. Barthel, D. J. Reilly, C. M. Marcus, M. P. Hanson, and A. C. Gossard, *Phys. Rev. Lett.* **103**, 160503 (2009).
- [34] J. R. Petta, A. C. Johnson, J. M. Taylor, E. A. Laird, A. Yacoby, M. D. Lukin, C. M. Marcus, M. P. Hanson, and A. C. Gossard, *Science* **309**, 2180 (2005).
- [35] J. Medford, J. Beil, J. M. Taylor, E. I. Rashba, H. Lu, A. C. Gossard, and C. M. Marcus, *Phys. Rev. Lett.* **111**, 050501 (2013).
- [36] E. A. Laird, J. M. Taylor, D. P. DiVincenzo, C. M. Marcus, M. P. Hanson, and A. C. Gossard, *Phys. Rev. B* **82**, 075403 (2010).
- [37] J. M. Taylor, V. Srinivasa, and J. Medford, *Phys. Rev. Lett.* **111**, 050502 (2013).
- [38] The specific detuning dependence of  $J$  within a Hubbard model is explained elsewhere [29] and remains phenomenological within this Letter.
- [39] These crossings require a change in electronic spin projections by 1, and hence we expect mixing on a time scale of  $T_2^* \approx 10$  ns due to uncontrolled nuclear spin fluctuations and the associated Overhauser gradients [4].
- [40] J. Medford, J. Beil, J. M. Taylor, S. D. Bartlett, A. C. Doherty, E. I. Rashba, D. P. DiVincenzo, H. Lu, A. C. Gossard, and C. M. Marcus, *Nat. Nanotechnol.* **8**, 654 (2013).
- [41] See Supplemental Material at <http://link.aps.org/supplemental/10.1103/PhysRevLett.119.227701> for additional leakage spectroscopy and details on extracting  $J$  from exchange oscillations.
- [42] E. Barnes, M. S. Rudner, F. Martins, F. K. Malinowski, C. M. Marcus, and F. Kuemmeth, *Phys. Rev. B* **93**, 121407 (R) (2016).